

# Rethinking Event-Based Object Detection through Representation-Level Temporal Aggregation and Model-Level Hypergraph Reasoning

Meisen Wang<sup>1</sup>, Hao Deng<sup>1</sup>, Wei Bao<sup>2</sup>, Ma Yuanxiao<sup>3</sup>, Chengjie Wang<sup>4</sup>,  
Zhiqiang Tian<sup>1</sup>, Shaoyi Du<sup>1</sup>, Siqi Li<sup>2</sup>

<sup>1</sup>Xi'an Jiaotong University   <sup>2</sup>Tsinghua University

<sup>3</sup>China Mobile System Integration   <sup>4</sup>Inner Mongolia Agricultural University

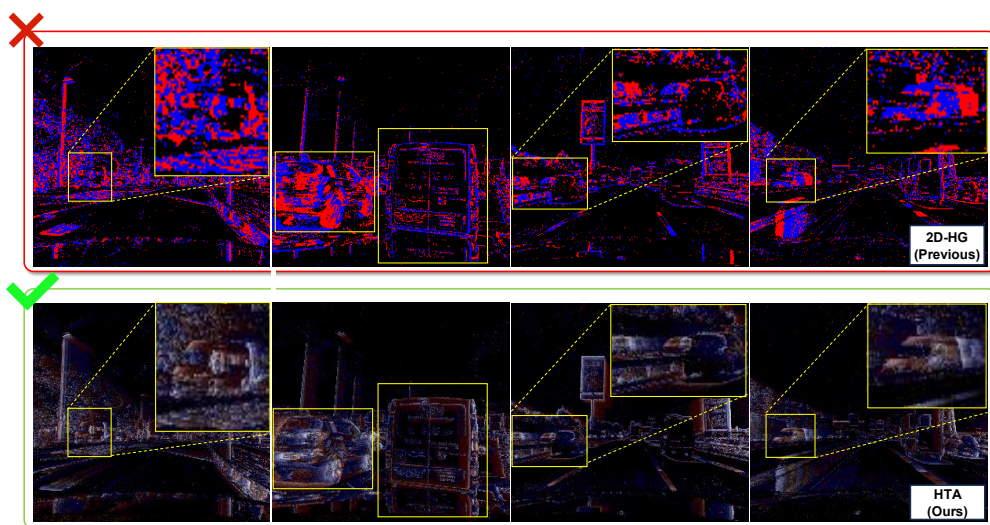


Figure 1: **Illustrative comparison between 2D Histogram (2D-HG) and Hierarchical Temporal Aggregation (HTA) representation.** HTA is one of our key contributions, encoding temporal event information into a compact pseudo-RGB format. Compared with 2D-HG, HTA produces cleaner object structures with reduced background noise. Yellow boxes highlight representative differences.

## Abstract

Event cameras provide microsecond-level temporal resolution, low latency, and high dynamic range, offering potential for perception under fast motion and challenging illumination conditions. However, existing Event-based Object Detection (EOD) methods face limitations at both the representation and model levels: prior event representations usually encode temporal information indirectly through redundant structures, while detection models struggle to explicitly aggregate fragmented event responses into coherent high-order object features. To address these limitations, we present **Event Dual Temporal-Relational Aggregation Detector (Ev-DTAD)**, a unified EOD framework that integrates representation-level temporal encoding with model-level temporal-hypergraph reasoning. Specifically, we introduce **Hierarchical Temporal Aggregation (HTA)**, a compact three-channel pseudo-RGB representation that explicitly embeds temporal information across intra- and inter-window events. To further enhance detection under sparse and fragmented event responses, we propose **Frequency-aware Hypergraph Temporal Fusion (FHTF)**, which refines multi-scale event features through temporal evolution modeling and high-order relational reasoning. Extensive experiments

on Gen1 (+0.8 mAP and 1.7× faster), 1Mpx/Gen4 (+0.5 mAP and 1.6× faster), and eTraM (+3.0 mAP and 2.0× faster) demonstrate that Ev-DTAD achieves a competitive accuracy–efficiency trade-off, validating the complementarity between compact temporal representation and temporal-hypergraph feature reasoning.

The code is available at: <https://github.com/meisenwang/Ev-DTAD>.

## 1 Introduction

Event cameras output asynchronous streams of brightness changes with microsecond-level temporal resolution, low latency, and high dynamic range, making them particularly attractive for perception in fast motion and challenging illumination conditions [21, 2, 11]. These advantages have motivated increasing interest in EOD for applications such as autonomous driving and robotics [23, 22, 8, 28, 13]. However, unlike conventional images, event streams are sparse, polarity-dependent, and temporally fragmented [11, 31]. Object-related event responses are often distributed across discontinuous events rather than captured in a complete spatial snapshot, making it challenging to preserve temporal structures and object features in a compact and informative representation [33, 12, 31].

Existing EOD studies can be grouped into two relatively independent research lines: *event representation and detection model design*. (i) *Event representation* aims to transform asynchronous events into more informative structures for effective detection [33, 3, 19, 26, 36, 45]. While these methods enhance access to event information, they capture temporal information indirectly through expanded temporal or feature dimensions [43, 12, 27], without explicitly embedding local event ordering or motion continuity into the representation, leading to redundancy. (ii) *Detection model design* focuses on strengthening the detector itself by modeling temporal dependencies over event-derived features [18, 14, 25, 46]. These methods improve temporal feature propagation and help accumulate sparse evidence over time, but they are less explicit in structuring discontinuous event responses into high-order object-level associations. This limitation is particularly pronounced in EOD, where object evidence is typically sparse and fragmented, arising from motion-induced brightness changes rather than dense region-level observations [11].

Motivated by these observations, we present **Event Dual Temporal-Relational Aggregation Detector (Ev-DTAD)**, a unified EOD framework that bridges event representation and detection model design through two complementary levels. Ev-DTAD compactly preserves discriminative event dynamics at the representation level and strengthens high-order feature association over sparse event responses at the model level. It introduces two key components: **Hierarchical Temporal Aggregation (HTA)** for compact temporal event encoding, and **Frequency-aware Hypergraph Temporal Fusion (FHTF)** for temporal-relational feature refinement.

The first component, **HTA**, addresses the compactness–expressiveness trade-off by encoding asynchronous events into a compact pseudo-RGB representation while preserving discriminative structures. Unlike prior methods that merely accumulate events or expand along temporal dimensions, HTA explicitly embeds temporal information into representation. Event information are aggregated at two temporal scales: intra-window aggregation captures local ordering and recent motion cues, while inter-window aggregation propagates reliable historical responses across adjacent windows, maintaining temporal continuity. The resulting three-channel representation encodes both instantaneous and historical temporal dynamics, preserving foreground motion structures and suppressing background noise, as illustrated in Fig. 1.

The second component, **FHTF**, addresses the fragmented nature of event features at the model level. Although HTA provides compact temporal encoding, object evidence in EOD remains sparse, incomplete, and distributed across time and scales. FHTF refines multi-scale event features by combining stateful temporal modeling with frequency-aware hypergraph reasoning. The temporal

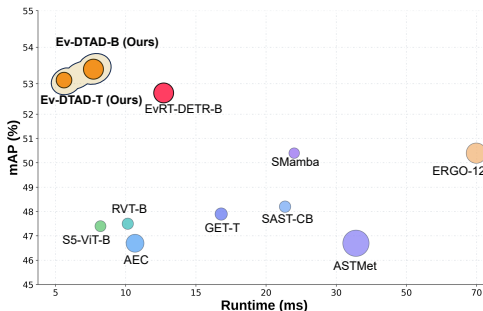


Figure 2: **Latency–accuracy comparison on Gen1**. Bubble area is proportional to the number of parameters. Our models achieve state-of-the-art accuracy while maintaining competitive inference speed.

branch propagates feature states across consecutive representations, while the hypergraph branch organizes discontinuous event responses into high-order structural contexts. Together, HTA and FHTF enable Ev-DTAD to combine compact event encoding with robust temporal-relational reasoning for event-based object detection.

We conduct experiments on Gen1 [8] (+0.8 mAP and  $1.7\times$  faster), 1Mpx/Gen4 [28] (+0.5 mAP and  $1.6\times$  faster), and eTraM [35] (+3.0 mAP and  $2.0\times$  faster). As illustrated in Fig. 2, Ev-DTAD establishes a competitive accuracy–efficiency trade-off, outperforming the strongest compared baselines in accuracy while reducing inference latency. These results validate the effectiveness of two-level EOD modeling for accurate and efficient EOD.

Our main contributions are summarized as follows:

1. We propose **HTA**, a compact three-channel event representation that hierarchically organizes intra-window motion ordering and inter-window reliable responses into a detector-friendly pseudo-RGB format, reducing redundant temporal encoding and explicitly embedding temporal dynamics at the representation level while preserving foreground structures.
2. We propose the **FHTF** module, a frequency-aware hypergraph temporal fusion module that performs high-order temporal-relational reasoning across event features at the model level, enhancing temporal robustness for sparse and temporally fragmented event streams.
3. We build **Ev-DTAD**, a two-level EOD framework that achieves a strong accuracy–efficiency trade-off on Gen1 (+0.8 mAP and  $1.7\times$  faster), 1Mpx/Gen4 (+0.5 mAP and  $1.6\times$  faster), and eTraM (+3.0 mAP and  $2.0\times$  faster), demonstrating the complementarity between compact temporal representation and feature-level temporal-relational refinement.

## 2 Related Work

**Event Representation.** A common strategy in EOD is to convert asynchronous event streams into dense grid-based representations, enabling image-style detection networks to process event data [11, 28, 14, 41, 25]. These representations provide efficient interfaces by accumulating event distributions, recent activity, or coarse temporal structures on regular grids, but they usually rely on fixed-window accumulation or temporal binning, which compresses fine-grained event dynamics into hand-crafted rasterizations. Recent methods improve event conversion by preserving richer spatiotemporal information. Peng et al. [26] introduce Hyper Histogram and Adaptive Event Conversion to encode polarity and temporal features with multi-channel tensors, while Zubić et al. [45] propose ERGO-12, a 12-channel event representation obtained by optimizing the ordering of event representation components. These studies confirm the importance of representation design, but also reveal a persistent limitation: richer temporal information is still largely retained through additional channels rather than explicit temporal encoding within the representation itself. As a result, existing representations face a trade-off between compactness and temporal expressiveness.

**Temporal modeling in Event-Based Object Detection.** Temporal modeling is another major line of EOD, aiming to exploit event sequences beyond single-window representations. Early recurrent detectors such as RED [28] introduce temporal memory, while ASTM-Net [18] adopts explicit memory for continuous aggregation. DMANet [36] leverages long- and short-term memory, and RVT [14] validates recurrent transformer-based modeling. GET [27] organizes events into structured tokens to model spatial, temporal, and polarity interactions, while later methods improve temporal modeling via temporal consistency learning [38], scene-adaptive sparse attention [25], state-space modeling [46], or detector adaptation [34]. Beyond dense-grid modeling, AEGNN [32] processes events as evolving spatio-temporal graphs, showing the potential of sparse structural modeling. These studies demonstrate the importance of model-level temporal reasoning for sparse and fragmented event observations. However, existing methods mainly emphasize temporal aggregation or pairwise structural modeling, leaving hypergraph-based high-order relations and frequency characteristics of event streams insufficiently explored for event feature refinement.

**Hypergraph-Based High-Order reasoning.** Hypergraphs naturally model high-order relations beyond pairwise interactions and have been widely studied in deep learning through hyperedge-based message passing and learnable propagation frameworks [10, 40, 17, 1, 16, 7]. In computer vision, hypergraph-based methods capture contextual and structural dependencies among visual regions [20, 15], and recent object detection studies show their effectiveness in modeling high-order

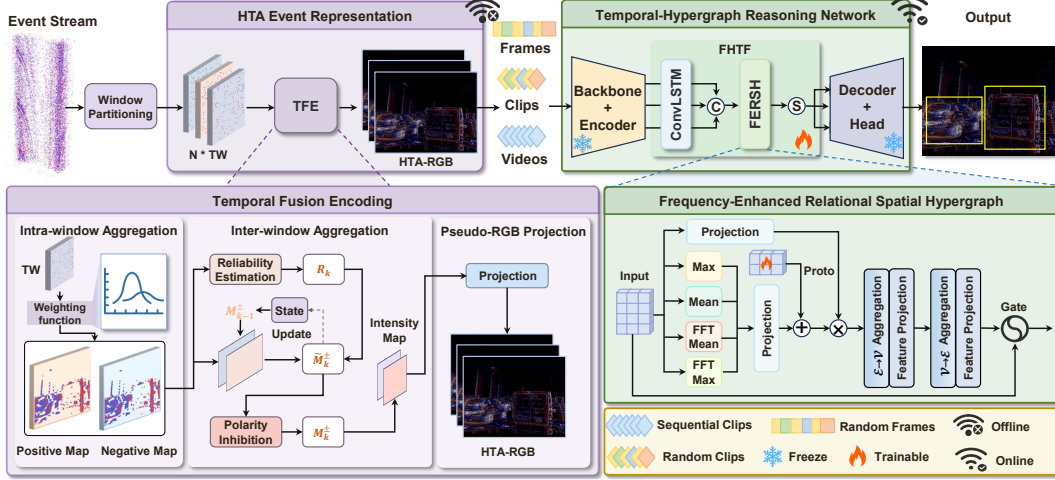


Figure 3: **Framework overview.** Ev-DTAD consists of two core components: offline HTA representation generation and the FHTF module. It first converts asynchronous events into compact HTA frames offline. Consecutive frames are grouped into clips/videos and fed into the network, where multi-scale features are extracted and refined by FHTF through temporal evolution and frequency-aware hypergraph reasoning. The refined features are finally decoded for object detection.

correlations among visual features [9]. Frequency-aware modeling has also been explored to enhance visual representations in the spectral domain [39, 6, 29, 30, 4]. However, existing hypergraph-based detection methods are mainly designed for frame-based inputs, leaving their potential in EOD underexplored. This motivates frequency-aware hypergraph reasoning to organize sparse and temporally evolving event features into high-order structural contexts.

### 3 Method

This section presents Ev-DTAD, a unified framework for EOD that combines representation-level temporal encoding with model-level temporal-hypergraph reasoning. We first introduce HTA, a compact event representation generated through hierarchical temporal aggregation, in Sec. 3.1. We then describe FHTF, which refines multi-scale event features through recurrent temporal propagation and frequency-aware hypergraph reasoning, in Sec. 3.2. Finally, Sec. 3.3 summarizes how the above two components are integrated into the complete Ev-DTAD detection pipeline, as illustrated in Fig. 3.

#### 3.1 HTA Event Representation

To explicitly encode temporal structures at the representation level, the asynchronous event stream is converted into a compact pseudo-RGB representation through hierarchical temporal aggregation across intra- and inter-window event dynamics. Formally, given an event stream

$$\mathcal{E} = \{e_i\}_{i=1}^N, \quad e_i = (x_i, y_i, t_i, p_i), \quad (1)$$

where  $x_i$  and  $y_i$  denote the spatial coordinates,  $t_i$  denotes the timestamp, and  $p_i \in \{-1, +1\}$  denotes the event polarity. We divide the asynchronous event stream into consecutive temporal windows  $\mathcal{W}_k = \{e_i \mid T_k \leq t_i < T_k + \Delta T\}$  of fixed length  $\Delta T$ .

**Intra-window temporal aggregation.** For each event  $e_i \in \mathcal{W}_k$ , a temporal weight is assigned as

$$\omega_i = \lambda + (1 - \lambda) \left( \frac{t_i - T_k}{\Delta T} \right)^{\gamma_t}, \quad (2)$$

where  $\lambda \in [0, 1]$  prevents early events from being fully suppressed, and  $\gamma_t$  controls the temporal recency bias. Positive and negative events are then separately accumulated with these weights to obtain window-level response maps  $P_k$  and  $N_k$ , preserving event activity and coarse temporal ordering compactly.

**Reliability-aware inter-window temporal aggregation.** To propagate temporal information across adjacent windows, two polarity-specific state maps,  $M_k^+$  and  $M_k^-$ , are maintained. Before updating them, we estimate the reliability of the current window response based on local activity intensity and polarity consistency. Using a local averaging operator  $\mathcal{B}(\cdot)$ , the reliability map is defined as

$$R_k = \text{clip}\left(\frac{\mathcal{B}(A_k)}{\mathcal{B}(A_k) + \tau} \cdot \frac{|\mathcal{B}(S_k)|}{\mathcal{B}(A_k) + \varepsilon}, 0, 1\right), \quad (3)$$

where  $A_k = P_k + N_k$  and  $S_k = P_k - N_k$ . Here,  $\tau$  is the activity normalization constant and  $\varepsilon$  is a small value to avoid division by zero.

Based on the local reliability, an adaptive decay rate is defined as

$$\kappa_k = \text{clip}(\kappa_0(1 + \alpha(1 - R_k)), \kappa_{\min}, \kappa_{\max}), \quad (4)$$

and update the two state maps by

$$\widetilde{M}_k^\pm = (1 - \kappa_k \Delta T)^b \odot M_{k-1}^\pm + c E_k^\pm, \quad (5)$$

where  $E_k^+ = P_k$  and  $E_k^- = N_k$ .  $\kappa_0$  is the base decay rate,  $\alpha$  is the modulation coefficient,  $b$  is the decay exponent, and  $c$  is the event injection coefficient and  $\kappa_{\min}$  and  $\kappa_{\max}$  are the minimum and maximum decay rates used to bound the decay strength.

To suppress simultaneous responses of opposite polarities at the same location, polarity-competitive inhibition is applied, followed by smooth saturation to bound the state magnitude:

$$M_k^+ = C \tanh\left(\frac{\max(\widetilde{M}_k^+ - \beta \widetilde{M}_k^-, 0)}{C}\right), \quad M_k^- = C \tanh\left(\frac{\max(\widetilde{M}_k^- - \beta \widetilde{M}_k^+, 0)}{C}\right), \quad (6)$$

where  $\beta$  is the inhibition coefficient and  $C$  is the state cap.

**Pseudo-RGB projection of temporally aggregated states.** After the above two-stage temporal aggregation, the final polarity states are converted into a pseudo-RGB image. A structural intensity map and a polarity bias map are first defined as:

$$\Pi_k = \frac{M_k^+ - M_k^-}{M_k^+ + M_k^- + \varepsilon}, \quad U_k = (1 - \eta) \max(M_k^+, M_k^-) + \eta |M_k^+ - M_k^-|. \quad (7)$$

A logarithmic compression is then applied to obtain the luminance term

$$Y_k = \frac{\log(1 + g U_k)}{\log(1 + g \sigma)}. \quad (8)$$

The final three-channel output is computed as

$$I_k = \left[ \text{clip}(Y_k + \mu \max(\Pi_k, 0), 0, 1), Y_k, \text{clip}(Y_k + \mu \max(-\Pi_k, 0), 0, 1) \right]^{\gamma_c}, \quad (9)$$

where  $g$  is the luminance gain,  $\sigma$  is the normalization scale,  $\eta$  balances dominant response and polarity difference,  $\mu$  controls color strength, and  $\gamma_c$  denotes the gamma parameter. Instead of stacking positive and negative histograms, HTA uses  $Y_k$  as shared structural luminance and injects polarity biases into the red and blue channels. Thus, the three channels compactly encode motion-induced structural intensity and polarity cues. After 8-bit quantization,  $I_k \in \mathbb{R}^{H \times W \times 3}$  denotes the pseudo-RGB representation for the  $k$ -th window.

Overall, HTA forms a temporally integrated state through hierarchical temporal aggregation rather than an isolated single-window snapshot, jointly preserving recent event responses, polarity-aware motion cues, and cross-window continuity in a compact three-channel representation.

### 3.2 FHTEF: Frequency-Hypergraph Temporal Fusion

To fully exploit the multi-scale spatiotemporal dynamics and high-order dependencies inherent in asynchronous event streams, the **FHTEF** module is proposed. It refines the multi-scale feature pyramid  $F_t = \{f_{t,i}\}_{i=1}^3$  by combining ConvLSTM-based local stateful temporal evolution with Frequency-Enhanced Relational Spatial Hypergraph, producing temporally coherent, relation-enhanced, and structurally robust event features before prediction.

**Stateful Temporal Evolution.** At each scale  $i$ , FHTF maintains a recurrent state to model the temporal evolution of event features without heavy spatiotemporal operators. To preserve pretrained spatial priors while injecting temporal dynamics, a residual gating mechanism is used:

$$\hat{f}_{t,i} = f_{t,i} + \alpha_i \cdot \Psi_i(f_{t,i}, \mathcal{M}_{t-1,i}), \quad (10)$$

where  $\Psi_i$  denotes the recurrent transition function,  $\mathcal{M}_{t-1,i}$  represents the hidden memory state propagated from the previous frame, and  $\alpha_i$  is a learnable gating parameter initialized to zero. This formulation ensures that temporal context is integrated seamlessly only where it provides discriminative temporal information.

**Frequency-Enhanced Relational Spatial Hypergraph (FERSH).** A key component of FHTF is the frequency-aware hypergraph refinement stage. Unlike pairwise self-attention, FHTF constructs latent hyperedges to capture high-order semantic and structural relations.

The hypergraph is defined over the spatially aligned multi-scale nodes  $X \in \mathbb{R}^{N \times C}$ . Since events are triggered by local brightness changes, object boundaries and motion-induced structures are often reflected in frequency-sensitive responses. These frequency-sensitive responses are used to guide the construction of hyperedges. Specifically, a Fast Fourier Transform (FFT) is applied over the feature sequence to extract spectral amplitude statistics:

$$c_{\text{spec}} = [\text{mean}(|\mathcal{F}(X)|), \max(|\mathcal{F}(X)|)]. \quad (11)$$

These spectral descriptors, combined with spatial global pooling statistics, modulate a learnable prototype matrix  $\mathbf{P} \in \mathbb{R}^{H \times d_k}$  to generate  $H$  frequency-aware hyperedge anchors.

A soft incidence matrix  $\mathcal{H} \in \mathbb{R}^{N \times H}$  models the association between spatial tokens and frequency-driven hyperedges. FHTF performs dual-hop message passing by aggregating node features into hyperedges for global context and broadcasting enriched hyperedge representations back to nodes for high-order refinement:

$$X_{\text{FHTF}} = X + \gamma \odot \Phi_{\text{broadcast}}(\mathcal{H} \cdot \Phi_{\text{agg}}(\mathcal{H}^\top X)), \quad (12)$$

where  $\Phi_{\text{agg}}$  and  $\Phi_{\text{broadcast}}$  denote the aggregation and redistribution projections, respectively, and  $\gamma$  serves as a channel-wise refinement gate. Through this frequency-aware hypergraph reasoning, FHTF module emphasizes structurally informative frequency patterns and improves the coherence of object-related event features.

### 3.3 Overall Ev-DTAD Framework

Building upon HTA and FHTF, Ev-DTAD forms a complete representation-to-detection framework for EOD. Asynchronous events are sliced into temporal windows, converted offline into compact HTA frames, and organized into clips for video-level detection. An RT-DETR-style detector with a PResNet backbone and encoder extracts multi-scale features, which are refined by FHTF through recurrent temporal propagation and frequency-aware hypergraph reasoning. A DETR-style query decoder then predicts object categories and bounding boxes. Training follows a two-stage protocol: a single-frame detector is first trained on HTA frames, followed by temporal refinement training on clips initialized from this checkpoint. During temporal training, RNN states are preserved across sequential clips/videos and reset for random clips to maintain temporal consistency. The model is optimized with Hungarian matching and standard detection losses, including classification,  $\ell_1$  box regression, and generalized IoU losses.

## 4 Experiments

### 4.1 Experimental Setup

**Datasets.** Ev-DTAD is evaluated on three representative EOD benchmarks: Gen1 [8], 1Mpx/Gen4 [28], and eTraM [35]. Gen1 provides low-resolution automotive recordings with sparse annotations, while 1Mpx/Gen4 contains higher-resolution driving scenes with denser annotations. eTraM further evaluates static traffic monitoring under diverse lighting and weather conditions. Together, these benchmarks enable a comprehensive evaluation across low-resolution automotive scenes, high-resolution dense traffic scenes, and static traffic monitoring scenarios, covering diverse spatial resolutions, annotation densities, scene layouts, and event acquisition settings.

Table 1: **Comparison on Gen1 and 1Mpx/Gen4.** Colors denote event representations. Runtime is measured in ms/frame. Best and second-best results are marked in **bold** and underline, respectively.

Method	Venue	Representation	Gen1		1Mpx/Gen4		Params (M)
			mAP (%)	Runtime (ms)	mAP (%)	Runtime (ms)	
ASTMNet [18]	TIP'22	Asynchronous Events	46.7	35.6	48.3	72.3	>100
AEC [26]	AAAI'23	Hyper Histogram	47.0	10.6	48.4	37.6	46.5
GET-T [27]	ICCV'23	Group Tokens	47.9	16.8	48.4	18.2	21.9
ERGO-12 [45]	ICCV'23	ERGO-12	50.4	69.9	40.6	100.0	59.6
SAST-CB [25]	CVPR'24	Voxel Grid	48.2	22.7	48.7	23.6	18.9
MAD-Det [5]	TIP'25	MAD	49.2	15.2	49.5	17.2	-
RVT-B [14]	CVPR'23	2D Histogram	47.2	10.2	47.4	11.9	18.5
S5-ViT-B [46]	CVPR'24	2D Histogram	47.4	8.2	47.2	<u>9.6</u>	17.5
SMamba [41]	AAAI'25	2D Histogram	50.4	24.0	49.3	26.0	16.7
SATE [44]	NeurIPS'25	2D Histogram	52.7	8.8	49.1	13.3	26.4
EvRT-DETR-B [34]	ICCV'25	2D Histogram	52.7	12.7	<u>50.1</u>	18.8	57.1
Ev-DTAD-T (ours)	-	HTA	<u>53.1</u>	<b>5.6</b>	48.6	<b>8.0</b>	35.2
Ev-DTAD-B (ours)	-	HTA	<b>53.5</b>	<u>7.6</u>	<b>50.6</b>	12.1	57.8

Table 2: **Comparison with SOTA methods on the traffic monitoring dataset eTraM.**

Method	Representation	mAP (%)	Runtime (ms)
SAST-CB [25]	Voxel Grid	30.0	24.4
RVT-B [14]	2D Histogram	29.5	11.9
S5-ViT-B [46]	2D Histogram	29.3	<u>10.9</u>
SMamba [41]	2D Histogram	32.6	25.2
Ev-DTAD-T (ours)	HTA	<u>35.3</u>	<b>8.3</b>
Ev-DTAD-B (ours)	HTA	<b>35.6</b>	12.3

Table 3: **Ablation study on the individual and joint contributions of the HTA event representation and the FHTF module.**

HTA	FHTF	mAP (%)	mAP <sub>50</sub> (%)	mAP <sub>75</sub> (%)
✗	✗	47.6	75.6	49.5
✓	✗	51.3	79.7	53.8
✗	✓	52.9	82.2	55.9
✓	✓	53.5	82.2	56.7

**Event Representations.** Following the standard event-to-frame protocol, we partition the asynchronous event stream into fixed 50 ms windows and convert each window into the proposed HTA representation. For Gen1, with an original resolution of  $240 \times 304$ , each representation is padded to  $256 \times 320$  for divisibility by 32 in the feature pyramid. For 1Mpx/Gen4 and eTraM, with original resolution  $720 \times 1280$ , representations are downsampled to  $360 \times 640$  by bilinear interpolation and padded to  $384 \times 640$ . This protocol follows prior work and enables fair computational comparison across datasets. For temporal modeling, consecutive windows are grouped into clips, with length 21 for Gen1 and 10 for 1Mpx/Gen4 and eTraM.

**Two-stage training.** Ev-DTAD is trained in two stages, with Ev-DTAD-T and Ev-DTAD-B denoting lightweight and base variants using PResNet-18 and PResNet-50 backbones, respectively. A single-frame detector is first trained for 400k iterations to learn stable spatial representations, after which the temporal refinement branch is trained for 200k iterations from the single-frame checkpoint. During temporal training, newly added temporal parameters are optimized, while the backbone, encoder, and most spatial layers remain frozen. The total batch size is 32 for single-frame training and 8 for temporal training. All experiments use a single NVIDIA RTX 3090 GPU.

## 4.2 Comparison with State-of-the-Art Methods

**Results on Gen1 and 1Mpx/Gen4.** Ev-DTAD is compared with representative state-of-the-art EOD methods on Gen1 and 1Mpx/Gen4 in Tab. 1. On Gen1, the accuracy-oriented Ev-DTAD-B achieves the best performance with **53.5% mAP**, outperforming EvRT-DETR-B by 0.8 mAP while being **1.7**× faster. Meanwhile, the lightweight Ev-DTAD-T reaches 53.1% mAP with the fastest inference speed of **5.6 ms**. On 1Mpx/Gen4, Ev-DTAD-B obtains the best result of **50.6% mAP**, improving over EvRT-DETR-B by 0.5 mAP while reducing inference latency by **1.6**×. Ev-DTAD-T further achieves the fastest runtime of **8.0 ms**, showing the scalability of the proposed design to high-resolution event streams. Compared with 2D Histogram-based methods and models using richer event representations, Ev-DTAD consistently delivers a stronger accuracy–efficiency trade-off, validating the effectiveness of compact HTA representation and frequency-aware temporal-hypergraph reasoning.

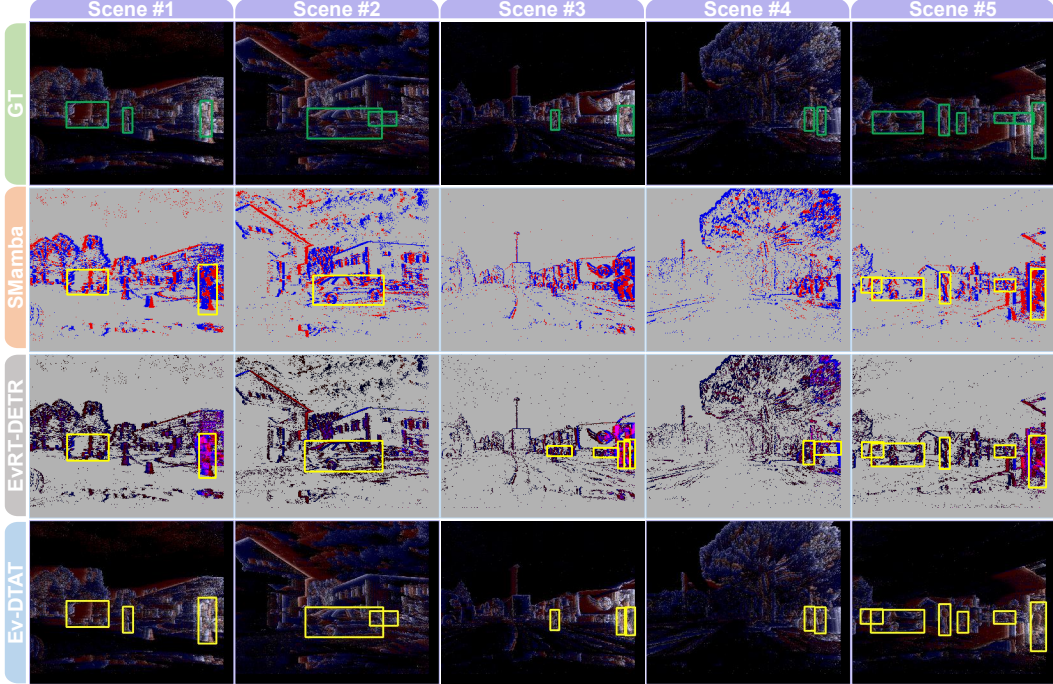


Figure 4: **Qualitative comparisons on Gen1.** Ev-DTAD achieves more accurate and robust detections than the baseline, reducing missed detections and improving localization in challenging scenes.

Table 4: **Ablation study on intra- and inter-window aggregation in HTA.**

Intra-Agg.	Inter-Agg.	mAP (%)	mAP <sub>50</sub> (%)
✗	✗	51.3	79.5
✓	✗	51.7	80.2
✗	✓	53.2	82.1
✓	✓	53.5	82.2

Table 5: **Ablation study on FHTF module, consisting of FERSH and ConvLSTM.**

FERSH	ConvLSTM	mAP (%)	Runtime (ms)	Params (M)
✗	✗	51.3	6.2	42.8
✓	✗	51.8	7.2	43.5
✗	✓	52.5	7.3	57.1
✓	✓	53.5	7.6	57.8

**Results on eTraM.** To evaluate cross-scenario generalization, Ev-DTAD is compared with recent EOD methods on eTraM in Tab. 2. eTraM differs from Gen1 and 1Mpx/Gen4 by using static traffic surveillance scenes with varied viewpoints, object scales, and illumination conditions. Ev-DTAD-B achieves **35.6% mAP**, outperforming SMamba by **3.0 mAP** while being **2.0×** faster. The lightweight Ev-DTAD-T obtains **35.3% mAP** with the fastest runtime of **8.3 ms**, maintaining almost the same accuracy as Ev-DTAD-B with further reduced latency. These results show that Ev-DTAD not only generalizes beyond automotive driving scenarios to static traffic monitoring settings, but also establishes a strong accuracy–efficiency trade-off across diverse EOD benchmarks.

### 4.3 Ablation Study

Unless otherwise specified, all ablation studies and component analyses in Sec. 4.3 and Sec. 4.4 are conducted on the Gen1 benchmark under the same evaluation protocol as the main comparison.

**Effectiveness of HTA and FHTF.** HTA and FHTF are first ablated in Tab. 3. Compared with the 2D-HG baseline without FHTF, HTA brings a +3.7 mAP improvement, showing the benefit of compact representation-level temporal encoding. FHTF brings a larger +5.3 mAP improvement over the same baseline, indicating the effectiveness of temporal-relational feature modeling. Combining HTA and FHTF achieves the best result of 53.5% mAP and improves mAP<sub>75</sub> by +7.2, validating their complementarity for both overall detection and stricter localization.

**Ablation on intra- and inter-window aggregation.** Tab. 4 analyzes the two aggregation levels in HTA. Compared with the variant without hierarchical aggregation, intra-window aggregation

Table 6: **Evaluation of the generalizability and effectiveness of HTA across different object detection architectures.**

Method	Backbone	2D-HG	HTA	$\Delta$ mAP
RT-DETR-B [42]	DETR	47.6	51.3	+3.7
D-FINE [24]	DETR	47.6	52.2	+4.6
RVT-B [14]	Transformer+RNN	47.2	47.7	+0.5
Ev-DTAD-B (ours)	DETR+RNN	52.7	53.5	+0.8

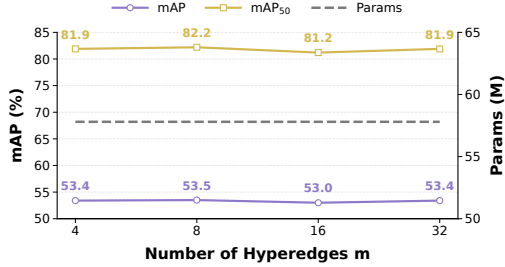


Figure 5: **Hyperedge sensitivity of FHTE.**

brings a +0.4 mAP improvement, while inter-window aggregation brings a +1.9 mAP improvement. Combining both achieves the best performance of 53.5% mAP and improves the no-aggregation variant by +2.2 mAP. These results show that intra-window aggregation captures local temporal evidence, while inter-window aggregation preserves temporal continuity across adjacent windows.

**Ablation on FHTE components.** Tab. 5 studies FERSH and ConvLSTM within FHTE. Starting from the HTA baseline without FHTE, FERSH brings a +0.5 mAP improvement, suggesting that frequency-aware hypergraph reasoning provides useful relational refinement. ConvLSTM brings a larger +1.2 mAP improvement, showing the importance of stateful temporal modeling. Combining FERSH and ConvLSTM achieves the best result of 53.5% mAP, indicating that high-order relational reasoning complements recurrent temporal aggregation.

#### 4.4 Further Analysis

**Generalizability of HTA.** To examine whether HTA is architecture-specific, it is evaluated across different object detection architectures in Tab. 6. The evaluated models include mainstream image-based detectors, i.e., RT-DETR-B [42] and D-FINE [24], as well as the representative event-based detector RVT-B [14]. Compared with the standard 2D-HG representation, HTA consistently improves detection performance across all architectures. In particular, it brings clear gains on mainstream DETR-based detectors, improving RT-DETR-B from 47.6% to 51.3% mAP and D-FINE from 47.6% to 52.2% mAP. This indicates that HTA can serve as a general event representation rather than a detector-specific preprocessing design.

We further observe relatively modest improvements when recurrent modeling is already present, e.g., +0.5 mAP on RVT-B and +0.8 mAP on Ev-DTAD-B. One possible explanation is that HTA has already encoded part of the temporal dynamics at the representation level, leaving less additional temporal information for RNN-based modules to further exploit. This indicates that stronger representation-level temporal encoding may reduce the dependence on recurrent modules and BPTT-based training in future EOD systems. Nevertheless, the consistent improvements across both image-style detectors and event-specific recurrent detectors demonstrate the generalizability of HTA.

**Hyperedge sensitivity.** The sensitivity of FHTE to the number of hyperedges  $m$  is analyzed in Fig. 5. When varying  $m$  from 4 to 32, performance remains stable, with mAP ranging from 53.0% to 53.5% and mAP<sub>50</sub> from 81.2% to 82.2%. Although the best result is obtained at  $m = 8$ , the differences are marginal and the parameter count remains unchanged at 57.8M. These results indicate that FHTE is robust to the choice of hyperedge number.

## 5 Conclusion

In this paper, we present Ev-DTAD, a unified framework that addresses EOD from two complementary levels: representation-level temporal event encoding and model-level temporal-hypergraph reasoning. Experiments on Gen1 (+0.8 mAP, 1.7× faster), 1Mpx/Gen4 (+0.5 mAP, 1.6× faster), and eTraM (+3.0 mAP, 2.0× faster) demonstrate a competitive accuracy–efficiency trade-off. Further analysis indicates that representation-level temporal encoding can complement model-level recurrent modeling, suggesting a promising direction for designing accurate and efficient EOD systems with reduced dependence on heavy recurrent training.

## References

- [1] Song Bai, Feihu Zhang, and Philip HS Torr. Hypergraph convolution and hypergraph attention. *Pattern Recognition*, 110:107637, 2021.
- [2] Christian Brandli, Raphael Berner, Minhao Yang, Shih-Chii Liu, and Tobi Delbruck. A 240x180 130 db 3  $\mu$ s latency global shutter spatiotemporal vision sensor. *IEEE Journal of Solid-State Circuits*, 49(10):2333–2341, 2014.
- [3] Marco Cannici, Marco Ciccone, Andrea Romanoni, and Matteo Matteucci. A differentiable recurrent surface for asynchronous event-based data. In *European Conference on Computer Vision*, pages 136–152. Springer, 2020.
- [4] Linwei Chen, Lin Gu, Dezhi Zheng, and Ying Fu. Frequency-adaptive dilated convolution for semantic segmentation. In *Proceedings of the IEEE/CVF Conference on Computer Vision and Pattern Recognition*, pages 3414–3425, 2024.
- [5] Nuo Chen, Boyang Li, Yingqian Wang, Xinyi Ying, Longguang Wang, Chushu Zhang, Yulan Guo, Miao Li, and Wei An. Motion and appearance decoupling representation for event cameras. *IEEE Transactions on Image Processing*, 34:5964–5977, 2025.
- [6] Lu Chi, Borui Jiang, and Yadong Mu. Fast fourier convolution. *Advances in Neural Information Processing Systems*, 33:4479–4488, 2020.
- [7] Eli Chien, Chao Pan, Jianhao Peng, and Olgica Milenkovic. You are allset: A multiset function framework for hypergraph neural networks. *arXiv preprint arXiv:2106.13264*, 2021.
- [8] Pierre De Tournemire, Davide Nitti, Etienne Perot, Davide Migliore, and Amos Sironi. A large scale event-based detection dataset for automotive. *arXiv preprint arXiv:2001.08499*, 2020.
- [9] Yifan Feng, Jiangang Huang, Shaoyi Du, Shihui Ying, Jun-Hai Yong, Yipeng Li, Guiguang Ding, Rongrong Ji, and Yue Gao. Hyper-yolo: When visual object detection meets hypergraph computation. *IEEE transactions on pattern analysis and machine intelligence*, 47(4):2388–2401, 2024.
- [10] Yifan Feng, Haoxuan You, Zizhao Zhang, Rongrong Ji, and Yue Gao. Hypergraph neural networks. In *Proceedings of the AAAI conference on artificial intelligence*, volume 33, pages 3558–3565, 2019.
- [11] Guillermo Gallego, Tobi Delbrück, Garrick Orchard, Chiara Bartolozzi, Brian Taba, Andrea Censi, Stefan Leutenegger, Andrew J Davison, Jörg Conradt, Kostas Daniilidis, et al. Event-based vision: A survey. *IEEE transactions on pattern analysis and machine intelligence*, 44(1):154–180, 2020.
- [12] Daniel Gehrig, Antonio Loquercio, Konstantinos G Derpanis, and Davide Scaramuzza. End-to-end learning of representations for asynchronous event-based data. In *Proceedings of the IEEE/CVF international conference on computer vision*, pages 5633–5643, 2019.
- [13] Mathias Gehrig, Willem Aarents, Daniel Gehrig, and Davide Scaramuzza. Dsec: A stereo event camera dataset for driving scenarios. *IEEE Robotics and Automation Letters*, 6(3):4947–4954, 2021.
- [14] Mathias Gehrig and Davide Scaramuzza. Recurrent vision transformers for object detection with event cameras. In *Proceedings of the IEEE/CVF conference on computer vision and pattern recognition*, pages 13884–13893, 2023.
- [15] Yan Han, Peihao Wang, Souvik Kundu, Ying Ding, and Zhangyang Wang. Vision hgnn: An image is more than a graph of nodes. In *Proceedings of the IEEE/CVF International Conference on Computer Vision*, pages 19878–19888, 2023.
- [16] Jing Huang and Jie Yang. Unignn: a unified framework for graph and hypergraph neural networks. *arXiv preprint arXiv:2105.00956*, 2021.
- [17] Jianwen Jiang, Yuxuan Wei, Yifan Feng, Jingxuan Cao, and Yue Gao. Dynamic hypergraph neural networks. In *Ijcai*, pages 2635–2641, 2019.

- [18] Jianing Li, Jia Li, Lin Zhu, Xijie Xiang, Tiejun Huang, and Yonghong Tian. Asynchronous spatio-temporal memory network for continuous event-based object detection. *IEEE Transactions on Image Processing*, 31:2975–2987, 2022.
- [19] Jianing Li, Xiao Wang, Lin Zhu, Jia Li, Tiejun Huang, and Yonghong Tian. Retinomorphic object detection in asynchronous visual streams. In *Proceedings of the AAAI Conference on Artificial Intelligence*, volume 36, pages 1332–1340, 2022.
- [20] Xi Li, Yao Li, Chunhua Shen, Anthony Dick, and Anton Van Den Hengel. Contextual hypergraph modeling for salient object detection. In *Proceedings of the IEEE international conference on computer vision*, pages 3328–3335, 2013.
- [21] Patrick Lichtsteiner, Christoph Posch, and Tobi Delbruck. A 240x180 130 db 3  $\mu$ s latency global shutter spatiotemporal vision sensor. *IEEE journal of solid-state circuits*, 43(2):566–576, 2008.
- [22] Ana I Maqueda, Antonio Loquercio, Guillermo Gallego, Narciso García, and Davide Scaramuzza. Event-based vision meets deep learning on steering prediction for self-driving cars. In *Proceedings of the IEEE conference on computer vision and pattern recognition*, pages 5419–5427, 2018.
- [23] Elias Mueggler, Henri Rebecq, Guillermo Gallego, Tobi Delbruck, and Davide Scaramuzza. The event-camera dataset and simulator: Event-based data for pose estimation, visual odometry, and slam. *The International journal of robotics research*, 36(2):142–149, 2017.
- [24] Yansong Peng, Hebei Li, Peixi Wu, Yueyi Zhang, Xiaoyan Sun, and Feng Wu. D-fine: Redefine regression task in detr as fine-grained distribution refinement. *arXiv preprint arXiv:2410.13842*, 2024.
- [25] Yansong Peng, Hebei Li, Yueyi Zhang, Xiaoyan Sun, and Feng Wu. Scene adaptive sparse transformer for event-based object detection. In *Proceedings of the IEEE/CVF conference on computer vision and pattern recognition*, pages 16794–16804, 2024.
- [26] Yansong Peng, Yueyi Zhang, Peilin Xiao, Xiaoyan Sun, and Feng Wu. Better and faster: Adaptive event conversion for event-based object detection. In *Proceedings of the AAAI Conference on Artificial Intelligence*, volume 37, pages 2056–2064, 2023.
- [27] Yansong Peng, Yueyi Zhang, Zhiwei Xiong, Xiaoyan Sun, and Feng Wu. Get: Group event transformer for event-based vision. In *Proceedings of the IEEE/CVF International Conference on Computer Vision*, pages 6038–6048, 2023.
- [28] Etienne Perot, Pierre De Tournemire, Davide Nitti, Jonathan Masci, and Amos Sironi. Learning to detect objects with a 1 megapixel event camera. *Advances in Neural Information Processing Systems*, 33:16639–16652, 2020.
- [29] Zequn Qin, Pengyi Zhang, Fei Wu, and Xi Li. Fcanet: Frequency channel attention networks. In *Proceedings of the IEEE/CVF international conference on computer vision*, pages 783–792, 2021.
- [30] Yongming Rao, Wenliang Zhao, Zheng Zhu, Jiwen Lu, and Jie Zhou. Global filter networks for image classification. *Advances in neural information processing systems*, 34:980–993, 2021.
- [31] Henri Rebecq, René Ranftl, Vladlen Koltun, and Davide Scaramuzza. High speed and high dynamic range video with an event camera. *IEEE transactions on pattern analysis and machine intelligence*, 43(6):1964–1980, 2019.
- [32] Simon Schaefer, Daniel Gehrig, and Davide Scaramuzza. Aegnn: Asynchronous event-based graph neural networks. In *Proceedings of the IEEE/CVF conference on computer vision and pattern recognition*, pages 12371–12381, 2022.
- [33] Amos Sironi, Manuele Brambilla, Nicolas Bourdis, Xavier Lagorce, and Ryad Benosman. Hats: Histograms of averaged time surfaces for robust event-based object classification. In *Proceedings of the IEEE conference on computer vision and pattern recognition*, pages 1731–1740, 2018.

- [34] Dmitrii Torbunov, Yihui Ren, Animesh Ghose, Odera Dim, and Yonggang Cui. Evrt-detr: Latent space adaptation of image detectors for event-based vision. In *Proceedings of the IEEE/CVF International Conference on Computer Vision*, pages 9812–9821, 2025.
- [35] Aayush Atul Verma, Bharatesh Chakravarthi, Arpitsinh Vaghela, Hua Wei, and Yezhou Yang. etram: Event-based traffic monitoring dataset. In *Proceedings of the IEEE/CVF conference on computer vision and pattern recognition*, pages 22637–22646, 2024.
- [36] Dongsheng Wang, Xu Jia, Yang Zhang, Xinyu Zhang, Yaoyuan Wang, Ziyang Zhang, Dong Wang, and Huchuan Lu. Dual memory aggregation network for event-based object detection with learnable representation. In *Proceedings of the AAAI Conference on Artificial Intelligence*, volume 37, pages 2492–2500, 2023.
- [37] Qirui Wang, Qi Guo, Yiding Sun, Junkai Yang, Dongxu Zhang, Shanmin Pang, and Qing Guo. Personalq: Select, quantize, and serve personalized diffusion models for efficient inference. *arXiv preprint arXiv:2603.22943*, 2026.
- [38] Ziyi Wu, Mathias Gehrig, Qing Lyu, Xudong Liu, and Igor Gilitschenski. Leod: Label-efficient object detection for event cameras. In *Proceedings of the IEEE/CVF conference on computer vision and pattern recognition*, pages 16933–16943, 2024.
- [39] Kai Xu, Minghai Qin, Fei Sun, Yuhao Wang, Yen-Kuang Chen, and Fengbo Ren. Learning in the frequency domain. In *Proceedings of the IEEE/CVF conference on computer vision and pattern recognition*, pages 1740–1749, 2020.
- [40] Naganand Yadati, Madhav Nimishakavi, Prateek Yadav, Vikram Nitin, Anand Louis, and Partha Talukdar. Hypergn: A new method for training graph convolutional networks on hypergraphs. *Advances in neural information processing systems*, 32, 2019.
- [41] Nan Yang, Yang Wang, Zhanwen Liu, Meng Li, Yisheng An, and Xiangmo Zhao. Smamba: Sparse mamba for event-based object detection. In *Proceedings of the AAAI Conference on Artificial Intelligence*, volume 39, pages 9229–9237, 2025.
- [42] Yian Zhao, Wenyu Lv, Shangliang Xu, Jinman Wei, Guanzhong Wang, Qingqing Dang, Yi Liu, and Jie Chen. Detrs beat yolos on real-time object detection. In *Proceedings of the IEEE/CVF conference on computer vision and pattern recognition*, pages 16965–16974, 2024.
- [43] Alex Zihao Zhu, Liangzhe Yuan, Kenneth Chaney, and Kostas Daniilidis. Unsupervised event-based learning of optical flow, depth, and egomotion. In *Proceedings of the IEEE/CVF conference on computer vision and pattern recognition*, pages 989–997, 2019.
- [44] Lin Zhu, Xiao Wang, Lizhi Wang, Hua Huang, et al. Rethinking scale-aware temporal encoding for event-based object detection. In *The Thirty-ninth Annual Conference on Neural Information Processing Systems*.
- [45] Nikola Zubić, Daniel Gehrig, Mathias Gehrig, and Davide Scaramuzza. From chaos comes order: Ordering event representations for object recognition and detection. In *Proceedings of the IEEE/CVF International Conference on Computer Vision*, pages 12846–12856, 2023.
- [46] Nikola Zubic, Mathias Gehrig, and Davide Scaramuzza. State space models for event cameras. In *Proceedings of the IEEE/CVF conference on computer vision and pattern recognition*, pages 5819–5828, 2024.

## Appendix

<b>A Additional Implementation Details</b> .....	13
A.1 Datasets .....	13
A.2 Baselines .....	14
A.3 Evaluation Metrics .....	15
A.4 Training & Inference Details .....	15
<b>B Additional Quantitative Results</b> .....	16
B.1 Overall Results on 1Mpx/Gen4 and eTraM .....	16
B.2 Class-wise Results .....	17
B.3 Video-wise Performance and Low-mAP Analysis on 1Mpx/Gen4 .....	18
<b>C Potential Societal Impact &amp; Limitations</b> .....	19
C.1 Societal Impact .....	19
C.2 Broader Implications .....	19
C.3 Limitations .....	19

## A Additional Implementation Details

### A.1 Datasets

We evaluate the proposed method on three representative event-based object detection benchmarks, including Gen1 [8], 1Mpx/Gen4 [28], and eTraM [35]. These datasets provide complementary evaluation settings for event-based object detection. Gen1 is a widely used low-resolution automotive benchmark and is suitable for evaluating detection robustness under sparse spatial observations. 1Mpx/Gen4 provides high-resolution event streams and dense annotations, making it appropriate for assessing the scalability of event representations and temporal modeling under richer spatial details. eTraM further extends the evaluation from ego-centric automotive driving to static traffic monitoring, where event distributions, camera viewpoints, object scales, and illumination conditions differ substantially from the driving benchmarks. Experiments on these three datasets allow us to evaluate the effectiveness, scalability, and cross-scenario generalization ability of our method. A summary of these datasets is provided in Tab. 7.

Table 7: **Summary of the event-based object detection datasets used in our experiments.**

Dataset	Resolution	Scenario	Classes	Main Purpose
Gen1 [8]	304 × 240	Automotive driving	2	Low-resolution robustness
1Mpx/Gen4 [28]	1280 × 720	Automotive driving	3	High-resolution scalability
eTraM [35]	1280 × 720	Static traffic monitoring	3	Cross-scenario generalization

**Gen1.** Gen1 [8] is one of the earliest large-scale benchmarks for event-based object detection. It contains more than 39 hours of automotive recordings captured by a Prophesee GEN1 event camera with a spatial resolution of 304 × 240. The recordings cover diverse driving scenes, including urban roads, highways, suburban areas, and countryside environments, under different weather and illumination conditions. The dataset provides manually annotated bounding boxes for two object categories, i.e., *car* and *pedestrian*, with annotations provided at 1, 2, or 4 Hz depending on the sequence. In total, Gen1 contains 255,781 bounding-box annotations, including 228,123 boxes for *car* and 27,658 boxes for *pedestrian*. Due to its relatively low spatial resolution and sparse event observations, Gen1 is particularly useful for evaluating whether an event representation can retain sufficient temporal and structural cues when the spatial information is limited. In our experiments, Gen1 serves as the primary benchmark for validating the effectiveness of compact temporal encoding and temporal-relational feature modeling under low-resolution event-based perception.

**1Mpx/Gen4.** 1Mpx/Gen4 [28] is a high-resolution event-based object detection dataset collected with a 1-megapixel event camera. It contains 14.65 hours of automotive recordings with a spatial resolution of  $1280 \times 720$ , including 11.19 hours for training, 2.21 hours for validation, and 2.25 hours for testing. The dataset provides bounding-box annotations at 60 Hz for three traffic-related categories: *pedestrian*, *two-wheeler*, and *car*. In total, it contains 25,846,825 bounding-box annotations, including 16,303,824 boxes for *car*, 8,429,932 boxes for *pedestrian*, and 1,113,069 boxes for *two-wheeler*. Compared with Gen1, 1Mpx/Gen4 provides much higher spatial resolution and denser annotations, introducing richer object structures while also increasing the computational burden of event representation and detection. This makes it an important benchmark for evaluating whether a method can scale from low-resolution event streams to high-resolution event perception.

**eTraM.** eTraM [35] is an event-based traffic monitoring dataset designed for static-camera traffic perception. Unlike Gen1 and 1Mpx/Gen4, which are collected from moving platforms in automotive driving scenarios, eTraM is captured from fixed viewpoints and focuses on traffic monitoring scenes. It contains over 10 hours of event data collected with a Prophesee EVK4 HD event camera at a spatial resolution of  $1280 \times 720$ . The dataset provides over 2 million 2D bounding-box annotations. While the original annotations cover eight fine-grained traffic-participant categories, we follow the official grouped annotation protocol and evaluate detection on three categories: *Pedestrian*, *Vehicle*, and *Micro-mobility*. eTraM covers diverse traffic scenarios, including intersections, roadways, and local streets, under challenging lighting and weather conditions such as nighttime, glare, overexposure, twilight, and rain. Since its static-camera viewpoint and event statistics differ substantially from ego-centric driving datasets, eTraM serves as a strong benchmark for evaluating cross-scenario generalization. In our experiments, it is used to verify whether the proposed method remains effective beyond standard automotive benchmarks.

These three datasets jointly provide a comprehensive evaluation protocol for event-based object detection. Gen1 evaluates robustness under low-resolution and sparse event observations; 1Mpx/Gen4 evaluates scalability to high-resolution event streams and dense annotations; and eTraM evaluates generalization to static traffic monitoring scenes. The consistent evaluation across these datasets demonstrates that the proposed method is not tailored to a single benchmark, but can effectively handle diverse event-based detection scenarios.

## A.2 Baselines

We compare Ev-DTAD with representative baselines from two aspects: state-of-the-art event-based object detection methods and detector-oriented architectures for representation generalization. The first group evaluates the overall accuracy–efficiency trade-off of Ev-DTAD against recent EOD methods, while the second group examines whether the proposed HTA representation can consistently improve different detector architectures.

**State-of-the-art EOD baselines.** We first compare Ev-DTAD with representative event-based object detection methods on Gen1, 1Mpx/Gen4, and eTraM. These methods cover several major paradigms in event-based detection:

- **Representation-oriented methods.** AEC [26] and ERGO-12 [45] mainly improve detection by designing richer event representations. They serve as important baselines for evaluating whether our compact HTA representation can achieve strong performance without relying on high-dimensional event encodings.
- **Token- and attention-based methods.** GET-T [27] and SAST-CB [25] model event streams through spatiotemporal tokens or sparse attention mechanisms. These methods provide comparisons for evaluating the effectiveness of our temporal-relational feature modeling.
- **Recurrent temporal methods.** ASTMNet [18] and RVT-B [14] introduce recurrent modeling to aggregate temporal information across event windows. They are included to compare Ev-DTAD with widely used temporal memory mechanisms in EOD.
- **State-space-based methods.** S5-ViT-B [46] and SMamba [41] explore state-space sequence modeling for efficient temporal aggregation. These recent methods are used to compare our frequency-aware temporal-hypergraph reasoning with another strong temporal modeling paradigm.
- **DETR-based event detector.** EvRT-DETR-B [34] adapts DETR-style detection to event-based data and serves as a strong end-to-end event detection baseline.

**Detector-oriented baselines.** In addition to comparing with EOD-specific methods, we evaluate HTA on different detector architectures to examine whether the proposed representation is architecture-specific. Specifically, we consider RT-DETR-B [42] and D-FINE [24], two representative end-to-end object detectors originally developed for frame-based detection, as well as RVT-B [14], a representative recurrent event-based detector. For each architecture, we compare the standard 2D Histogram representation with the proposed HTA representation under the same detector setting. This directly evaluates whether HTA can serve as a general event representation rather than a preprocessing design tailored to Ev-DTAD.

The selected baselines cover both specialized EOD methods and general detector architectures, allowing us to evaluate Ev-DTAD from two complementary aspects: its competitiveness against recent event-based detectors and the generalizability of HTA across different detection backbones.

### A.3 Evaluation Metrics

We evaluate detection performance using standard object detection metrics based on bounding-box overlap. The primary metric is mean Average Precision (mAP), which follows the COCO-style evaluation protocol and averages AP over multiple Intersection-over-Union (IoU) thresholds from 0.50 to 0.95 with a step size of 0.05. Formally, it can be written as

$$\text{mAP} = \frac{1}{10} \sum_{\tau \in \{0.50, 0.55, \dots, 0.95\}} \text{AP}_{\tau}, \quad (13)$$

where  $\text{AP}_{\tau}$  denotes the average precision computed under the IoU threshold  $\tau$ . This metric jointly reflects classification accuracy and localization quality, and is therefore used as the main metric in our experiments.

In addition to mAP, we report the following metrics to provide a more comprehensive evaluation:

- **mAP<sub>50</sub>.**  $\text{mAP}_{50}$  measures AP at an IoU threshold of 0.50. It is a relatively tolerant metric and mainly reflects whether objects can be correctly detected with approximate localization.
- **mAP<sub>75</sub>.**  $\text{mAP}_{75}$  measures AP at an IoU threshold of 0.75. Compared with  $\text{mAP}_{50}$ , it imposes a stricter requirement on bounding-box localization and better reflects precise localization quality.
- **Runtime.** Runtime measures the average inference latency per frame and is reported in milliseconds. It is used to evaluate the practical efficiency of different methods during inference.
- **Params.** The number of parameters measures the model size and reflects the storage and memory cost of each detector.
- **FLOPs.** Floating-point operations estimate the computational complexity of a model. We report FLOPs when applicable to compare the computational cost of different methods.

These metrics allow us to evaluate both detection accuracy and efficiency, providing a comprehensive view of the accuracy–efficiency trade-off of different methods.

### A.4 Training & Inference Details

**Input configurations.** We use dataset-specific input resolutions to preserve the original event geometry while satisfying the divisibility requirement of the feature pyramid. The detailed input configurations are summarized in Tab. 8. For Gen1, we only apply padding to the original event canvas without resizing. For 1Mpx/Gen4 and eTraM, we first downsample the original frames by a factor of 2 and then pad them to the final input resolution. The same input sizes are used during both training and inference.

Table 8: **Dataset-specific input configurations.**

Dataset	Original Canvas	Preprocessing	Input Size	Clip Length
Gen1	240 × 304	Padding only	256 × 320	21
1Mpx/Gen4	720 × 1280	Downsample + padding	384 × 640	10
eTraM	720 × 1280	Downsample + padding	384 × 640	10

**Data augmentation and sampling.** During training, we apply horizontal flipping, random rotation, affine translation, scaling, shearing, and random erasing. For video training, geometric augmentations are applied consistently to all frames within the same clip to preserve temporal alignment, while random erasing is applied at the frame level. During evaluation, only deterministic resizing and padding are used.

For frame-based training, individual frames are sampled and unlabeled frames are skipped. For video-based training, we use both sequential video clips and randomly sampled clips. Fully unlabeled clips are skipped during training, while unlabeled frames inside a valid clip are retained as temporal context. During video evaluation, unlabeled frames are not skipped, so that the temporal memory can be continuously maintained across each video.

**Two-stage training protocol.** We adopt a two-stage training protocol. In the first stage, a frame-based RT-DETR detector is trained from scratch on individual HTA frames to establish strong spatial detection capability. This stage optimizes the backbone, encoder, and decoder under standard frame-level supervision.

In the second stage, the video detector is initialized from the EMA weights of the trained frame detector, and temporal modeling modules are introduced to exploit sequential event information. During this stage, the pretrained spatial detection components are largely kept fixed, while the temporal modules are optimized to aggregate information across consecutive event frames. This design decouples spatial detection learning from temporal feature modeling, enabling the video model to inherit robust frame-level representations while focusing on temporal aggregation and refinement.

Table 9: **Main training configurations.**

Stage	Model	Batch	Epochs	Iters/Epoch	Trainable Parts
Frame	RT-DETR-T	32	400	1000	Backbone, encoder, decoder
Frame	RT-DETR-B	32	400	1000	Backbone, encoder, decoder
Video	Ev-DTAD-T	8	200	1000	Temporal modules
Video	Ev-DTAD-B	8	200	1000	Temporal modules

The main training configurations are summarized in Tab. 9. For computationally controlled training, each epoch is defined as 1000 optimization iterations rather than a full pass over all training samples. This setting standardizes the optimization budget across datasets and training stages, since the number of available frames or clips varies substantially across Gen1, 1Mpx/Gen4, and eTraM, and video sampling further depends on clip construction. It also makes validation, checkpointing, and learning-rate scheduling comparable under a fixed iteration-based training budget.

**Model and loss.** The detector follows an RT-DETR-style architecture with a PResNet backbone. We use PResNet-18 for Ev-DTAD-T and PResNet-50 for Ev-DTAD-B. The transformer encoder takes multi-scale features with strides of [8, 16, 32], and the decoder uses 300 object queries. For video-based detection, the model further introduces ConvLSTM-based temporal encoding on multi-scale feature maps, followed by temporal query refinement.

We use Hungarian matching for label assignment. The training loss consists of Varifocal Loss, L1 bounding-box loss, and GIoU loss, with weights 1, 5, and 2, respectively.

## B Additional Quantitative Results

In this section, we provide additional quantitative results to further analyze the performance of Ev-DTAD. We first report the overall test results on 1Mpx/Gen4 and eTraM, followed by class-wise results on Gen1, 1Mpx/Gen4, and eTraM. Finally, we present video-wise results on 1Mpx/Gen4 and analyze representative low-mAP videos to better understand the remaining evaluation gap.

### B.1 Overall Results on 1Mpx/Gen4 and eTraM

We first present the overall test results on 1Mpx/Gen4 and eTraM. These two datasets provide complementary evaluation settings: 1Mpx/Gen4 evaluates high-resolution event-based object detection in ego-centric driving scenes, while eTraM evaluates cross-scenario generalization in static traffic moni-

toring scenes. As shown in Fig. 6 and Fig. 7, Ev-DTAD achieves a competitive accuracy–efficiency trade-off on both datasets.

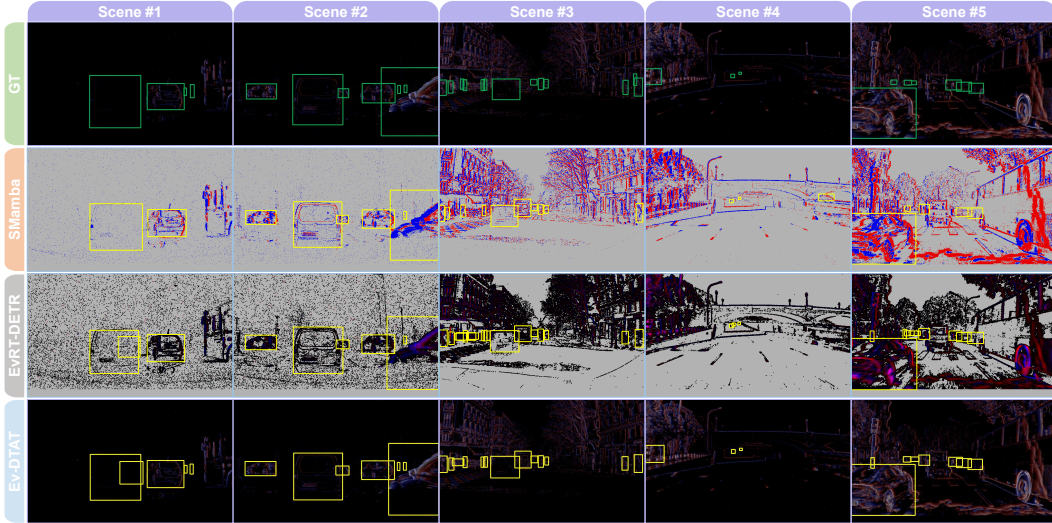


Figure 6: **Additional test results on 1Mpx/Gen4.** We report the detection performance of Ev-DTAD on the high-resolution driving benchmark.

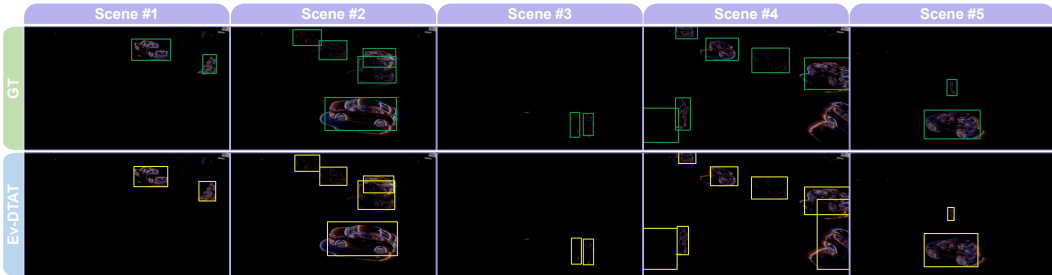


Figure 7: **Additional test results on eTraM.** We report the detection performance of Ev-DTAD on the static traffic monitoring benchmark.

## B.2 Class-wise Results

To further analyze the behavior of Ev-DTAD across object categories, we report class-wise AP on Gen1, 1Mpx/Gen4, and eTraM. Gen1 evaluates *car* and *pedestrian*; 1Mpx/Gen4 evaluates *pedestrian*, *two-wheeler*, and *car*; eTraM follows the official grouped protocol with *Pedestrian*, *Vehicle*, and *Micro-mobility*. The results are summarized in Tab. 10.

Table 10: **Class-wise AP of Ev-DTAD-T on Gen1, 1Mpx/Gen4, and eTraM.**  $\times$  indicates that the corresponding category is not evaluated in the dataset.

Dataset	Car	Pedestrian	Two-wheeler	Vehicle	Micro-mobility	mAP
Gen1	67.6	38.6	$\times$	$\times$	$\times$	53.1
1Mpx/Gen4	64.1	31.7	50.1	$\times$	$\times$	48.6
eTraM	$\times$	29.1	$\times$	52.0	24.9	35.3

The class-wise results show that Ev-DTAD-T performs consistently well on vehicle-related categories, achieving 67.6 AP on *car* in Gen1, 64.1 AP on *car* in 1Mpx/Gen4, and 52.0 AP on *Vehicle* in eTraM. This indicates that the proposed compact temporal representation and temporal-hypergraph modeling effectively preserve stable object structures for larger and more frequently observed traffic participants.

For smaller and more challenging categories, the performance is lower but still meaningful: Ev-DTAD-T obtains 38.6 AP on *pedestrian* in Gen1, 31.7 AP on *pedestrian* in 1Mpx/Gen4, and 29.1 AP on *Pedestrian* in eTraM. The relatively lower AP on pedestrians and micro-mobility objects suggests that these categories remain more sensitive to sparse event responses, small object scale, and fragmented motion boundaries. On 1Mpx/Gen4, the 50.1 AP on *two-wheeler* further shows that Ev-DTAD-T can capture intermediate-scale dynamic objects, while the 24.9 AP on *Micro-mobility* in eTraM highlights the difficulty of detecting small and diverse objects in static traffic monitoring scenes.

### B.3 Video-wise Performance and Low-mAP Analysis on 1Mpx/Gen4

Since 1Mpx/Gen4 contains diverse driving sequences with different motion patterns, object densities, and annotation conditions, we further report video-wise mAP to analyze performance variations across sequences. The video-wise results are summarized in Tab. 11. This video-level evaluation helps identify challenging sequences that may be hidden by dataset-level average performance.

Table 11: Video-wise detection results of Ev-DTAD-B on 1Mpx/Gen4.

Rank	Video	mAP	mAP <sub>50</sub>	mAP <sub>75</sub>
1	2019-02-19_001_td_1098500000_1158500000	66.6	85.3	72.4
2	2019-06-21_001_671500000_731500000	61.1	87.7	76.1
3	2019-06-17_test_01_000_1891500000_1951500000	60.1	93.9	58.3
...	...	...	...	...
118	2019-06-17_test_02_000_3599500000_3659500000	12.8	25.0	11.5
119	2019-06-17_test_02_000_3782500000_3842500000	12.4	29.7	9.3
120	2019-06-17_test_02_000_3660500000_3720500000	9.4	22.5	6.2

Based on the video-wise results in Tab. 11, we further inspect the videos with the lowest mAP scores. As shown in Fig. 8, several low-scoring sequences contain fast-moving objects, where the annotations are occasionally spatially misaligned with the event responses. In these cases, the predicted boxes can be visually closer to the apparent object locations in the event representation, but still receive lower scores due to the mismatch with the annotated boxes. Moreover, some erroneous annotations are still visible in the visualization, suggesting that imperfect label filtering may also affect the video-wise evaluation results.

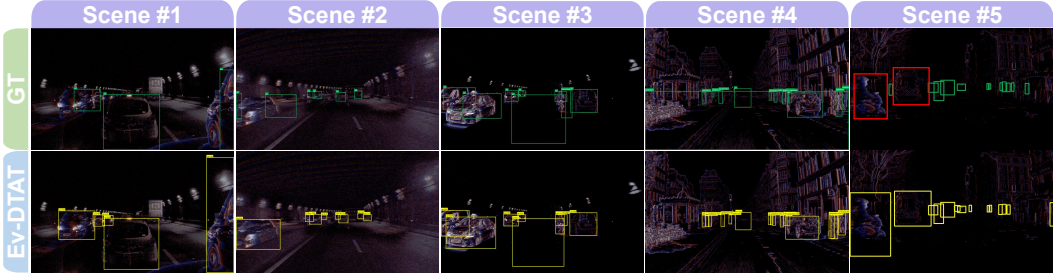


Figure 8: **Qualitative visualization of representative low-mAP Gen4 videos.** Red boxes indicate objects that are visually detected by our model but missing in the ground-truth annotations. Zoom in for details.

This observation suggests that video-level evaluation can reveal dataset-specific challenges that are not fully reflected by average mAP. For fair comparison with prior methods, our quantitative evaluation strictly follows the official annotations and filtering protocol, without manually modifying the filtering criteria. Nevertheless, Fig. 8 reveals several annotation-related issues in representative low-mAP sequences:

1. **Spatial annotation misalignment.** As shown in Scenes 1–3, some annotations in high-speed motion scenes are spatially misaligned with the corresponding event responses, causing visually reasonable predictions to receive lower scores.
2. **Erroneous boxes.** As shown in Scene 4, a small number of erroneous boxes are not properly removed by the official filtering protocol.
3. **Missing ground-truth annotations.** As shown in Scene 5, some objects are not annotated in the ground truth, while our model still detects them correctly according to the visual evidence.

These observations indicate that annotation alignment, box filtering, and missing annotations remain important factors for reliable evaluation in event-based detection benchmarks. Future work may explore motion-aware annotation refinement and more rigorous filtering protocols for high-speed event streams.

## C Potential Societal Impact & Limitations

### C.1 Societal Impact

The proposed Ev-DTAD framework has the potential to benefit a range of safety-critical and real-time perception applications that rely on event-based sensing. In particular, event cameras offer high temporal resolution, low latency, and high dynamic range, making them well suited for challenging scenarios such as high-speed motion, low-light environments, and scenes with strong illumination changes. By improving detection performance under such conditions, Ev-DTAD can contribute to more reliable perception in applications including autonomous driving, robotics, and intelligent transportation systems.

In addition, the proposed compact temporal encoding and efficient temporal modeling reduce redundant computations in event representation, which may help lower the computational cost compared with dense frame-based processing. This property is beneficial for deployment on resource-constrained platforms such as edge devices, where energy efficiency and real-time processing are critical.

### C.2 Broader Implications

Beyond the direct performance improvements, our analysis reveals several broader implications for event-based object detection benchmarks and evaluation protocols. In particular, the video-wise analysis on 1Mpx/Gen4 shows that dataset-level mAP may not fully reflect detection quality in certain scenarios. For example, in high-speed motion sequences, we observe that some annotations are spatially misaligned with the corresponding event responses, leading to cases where visually accurate predictions receive lower evaluation scores.

Moreover, we find that a small number of erroneous bounding boxes are not properly filtered by the official evaluation protocol. Although such cases are relatively rare, they can still affect video-level metrics and introduce additional evaluation noise. These observations suggest that both annotation alignment and box filtering play an important role in reliable benchmarking for event-based detection.

More generally, our results highlight the importance of complementary evaluation perspectives, such as video-wise analysis and qualitative inspection, in addition to aggregate metrics like mAP. Future research may further explore motion-aware annotation refinement, temporally consistent labeling strategies, or more rigorous filtering protocols to improve the reliability of evaluation under high-speed event streams.

At the same time, as event-based perception systems become more capable and widely deployed, there is a potential risk of misuse in applications such as large-scale surveillance. This underscores the need for appropriate guidelines and responsible use of such technologies.

### C.3 Limitations

Despite the effectiveness of Ev-DTAD, several limitations remain. First, the performance of the proposed method depends on the quality of the event representation. In scenarios with extremely

sparse or noisy event streams, the constructed HTA representation may not fully capture the underlying object structure, which can degrade detection performance.

Second, the two-stage training strategy introduces additional training complexity compared with end-to-end approaches. Although it helps stabilize optimization and improve performance, it requires careful coordination between the frame-based and video-based stages.

Third, while the proposed temporal modeling improves performance in dynamic scenes, it also introduces additional computational overhead, especially for high-resolution inputs such as 1Mpx/Gen4. This may limit scalability in real-time applications with strict latency constraints. One promising future direction is to explore quantization-based model compression and efficient deployment strategies, which may further reduce the computational cost of Ev-DTAD and facilitate its integration with large models [37].

Finally, similar to other supervised methods, the model may face challenges when generalizing to unseen environments with significantly different motion patterns or event characteristics. Exploring more robust representations, adaptation strategies, and efficient large-model-assisted event understanding remains an important direction for future work.